Check for updates

ASME Journal of Engineering for Gas Turbines and Power
Online journal at:
https://asmedigitalcollection.asme.org/gasturbinespower

Comparative Study of Hydrogen Addition Effects on Flame Stability and Pollutant Emissions in Jet-A1 and Sustainable Aviation Fuel/Jet-A1 Lean Lifted Spray Flames

Samarjeet Singh[1]
Engler-Bunte-Institute,
Division of Combustion Technology,
Karlsruhe Institute of Technology,
Karlsruhe 76131, Germany
e-mail: samarjeet.singh@kit.edu

Fabian P. Hagen
Engler-Bunte-Institute,
Division of Combustion Technology,
Karlsruhe Institute of Technology,
Karlsruhe 76131, Germany

Stefan R. Harth
Engler-Bunte-Institute,
Division of Combustion Technology,
Karlsruhe Institute of Technology,
Karlsruhe 76131, Germany

Dimosthenis Trimis
Engler-Bunte-Institute,
Division of Combustion Technology,
Karlsruhe Institute of Technology,
Karlsruhe 76131, Germany

Understanding the combustion characteristics of sustainable aviation fuel (SAF) and conventional fuel spray flames with hydrogen (H_2) mixtures is essential for enabling the transition from fossil fuels to cleaner aircraft propulsion. This study investigates flame stabilization and pollutant emissions in an innovative, fuel-flexible combustor fueled by Jet-A1, SAF, and H_2 under atmospheric pressure and elevated air inlet temperatures. A new nozzle, based on the "low swirl" lean-lifted flame concept, was developed to promote high premixing, significantly reducing NO_x emissions and minimizing flashback risk compared to conventional swirl-stabilized flames. The design promotes higher flame lift-off heights (LOH), enabling stable operation at increased H_2 content. Jet-A1 and SAF/Jet-A1 blend are injected through a centrally mounted hollow-cone atomizer, and H_2 is supplied via injectors arranged circumferentially around the prefilmer. Flame structure, lift-off height, and flame width were characterized using high-speed OH^* chemiluminescence imaging, and pollutant emissions were measured with an exhaust gas analyzer. The study compares flame behavior and pollutant emissions with and without H_2 addition in Jet-A1/air and SAF/Jet-A1/air lean lifted spray flames. The influence of H_2 addition on the lean blowout (LBO) behavior of the combustor is also assessed for both fuels. Overall, a comprehensive experimental campaign investigates key parameters, such as air inlet temperature and hydrogen blending ratio. The comparison of H_2 addition in Jet-A1 and SAF/Jet-A1 spray flames provides beneficial insights for the design and optimization of next-generation fuel-flexible aero-engines.
[DOI: 10.1115/1.4072618]

Keywords: hydrogen combustion, Jet-A1, SAF, fuel flexibility, pollutant emissions, gas turbine

1 Introduction

Aviation is one of the fastest-growing global transport sectors and is currently undergoing a paradigm shift driven by the urgent need to mitigate its environmental impact. Jet-A1, a kerosene-based aviation fuel produced under stringent international specifications, remains the predominant fuel for commercial turbine aircraft due to its high energy density, proven safety record, and extensive compatibility with existing infrastructure. However, combustion of Jet-A1 contributes approximately 2% of global CO_2 emissions [1,2], and projections indicate that this share could rise to nearly 5% by 2050 without intervention [3]. Therefore, the rapid development and deployment of sustainable combustion technologies for low-carbon or carbon-neutral alternatives is of utmost importance for achieving aviation's 2050 net-zero goals.

In this regard, two alternative pathways have gained prominence: the implementation of drop-in sustainable aviation fuels (SAFs) and the advancement of carbon-free fuels such as hydrogen (H_2). These strategies represent distinct routes toward lower-emission aviation. SAFs provide a near-term solution for reducing carbon footprint [4], whereas H_2 represents a longer-term transition toward zero-carbon combustion [5]. Derived from renewable or waste-based feedstocks, SAF is compatible with existing aircraft engines and infrastructure [6] and can reduce life-cycle CO_2 emissions by up to 94% relative to Jet-A1 [7]. Certified under ASTM D7566, managed by the American Society for Testing and Materials in the U.S., SAF can be blended up to 50% with Jet-A1. But global production of SAF

Turbo Expo: Turbomachinery Technical Conference & Exposition (GT2026), June 15–19, 2026. GT2026.
[1]Corresponding author.
Manuscript received May 5, 2026; final manuscript received May 12, 2026; published online September 10, 2026. Editor: Jerzy T. Sawicki.

Copyright © 2026 by ASME; reuse license CC-BY 4.0

Downloaded from asmedigitalcollection.asme.org/gasturbinespower/article-pdf/148/12/121009/7635651/gtp-26-1251.pdf by KIT Library user on 11 November 2026

remains limited, highlighting the need for further research on its combustion performance and scalability. In parallel, H_2 offers approximately 2.8 times the energy per unit mass of aviation kerosene [8] and, when burned, produces up to 90% lower NO_x emissions under optimized conditions [9]. Nonetheless, its low volumetric energy density, which necessitates larger storage tanks, together with ongoing challenges in production, storage, and handling, continues to hinder widespread adoption [10].

Fuel-flexible systems offer a bridge to low-carbon aviation by enabling the use of conventional Jet-A1, drop-in SAFs, and H_2 with minimal change in existing engine architectures [11,12]. Such systems can lower both local pollutant emissions in the vicinity of airports and overall flight emissions, achieving these benefits without restricting flight range or operability. Their capability to operate interchangeably on drop-in SAFs, H_2, and conventional Jet-A1 offers operational flexibility and supply-chain resilience, making fuel-flexible technologies an attractive near- to mid-term option for accelerating the adoption of cleaner aviation fuels. Indeed, several experimental [13–19] and theoretical [20–23] investigations have contributed significantly toward the dual fuel operation of H_2 and conventional aviation fuels.

Despite the promise of fuel-flexible operation, integrating alternative fuels such as drop-in SAFs with H_2 addition introduces substantial combustion challenges. On one side, SAF and Jet-A1 are complex multicomponent fuels with differing volatility and evaporation characteristics, leading to preferential evaporation effects that remain insufficiently understood and difficult to incorporate into current combustor design methodologies [24]. On the other side, the markedly different physical and chemical properties of H_2-rich fuel, particularly their high reactivity and fast flame speed, prevent direct application of conventional combustor designs, as these mixtures can shift flame anchoring behavior and, in extreme cases, lead to flashback [25]. As a result, designing fuel-flexible combustors that are simultaneously flashback-resistant, operationally stable, and capable of low emissions remains a major technical challenge for next-generation aviation propulsion systems. To the best knowledge of the authors, no prior studies have systematically addressed the challenges of achieving stable combustion ranging from pure SAF/Jet-A1 fuel to pure H_2 through intermediate fuel splits, under engine-relevant conditions.

This study examines the effects of H_2 addition on flame behavior, lean blowout (LBO) limits, and pollutant emissions of Jet-A1 and SAF/Jet-A1 blend lean lifted spray flames in a novel low-swirl combustor. The burner employs Jet-A1 or SAF/Jet-A1 fuels through an airblast atomizer, with H_2 injected in a jet-in-crossflow configuration, operating at elevated air inlet temperatures (T_{air}) and atmospheric pressure. This investigation addresses critical knowledge gaps related to the practical implementation of H_2 in dual-fuel systems employing conventional jet fuels or SAF/Jet-A1 blend. Specifically, the study analyzes flame shape variations with and without H_2 addition (up to 100%) in Jet-A1 and SAF/Jet-A1 spray flames and compares lift-off heights (LOH) and LBO limits across different fuel mixtures. Finally, the effects of varying H_2 blends on NO_x and CO emissions are quantified for both Jet-A1 and SAF/Jet-A1 flames.

2 Experimental Setup and Measurements

2.1 Combustion Facility. Experiments were conducted on a laboratory-scale fuel-flexible combustor designed to investigate lean lifted spray flames of Jet-A1 and SAF/Jet-A1 with H_2 addition. The experimental setup, shown in Fig. 1(*a*), consists of an air supply plenum, a quartz-enclosed combustion chamber for full optical access, and an open exhaust leading to an extraction system. Compressed air is preheated to 673 K using electrical heaters before entering the plenum, which incorporates a flow straightener to ensure uniform inlet conditions. The combustion chamber has a square cross section of 100 × 100 mm^2 and extends 460 mm above the burner exit. The nozzle with an effective area of 380 mm^2, is designed to enable dual-fuel operation.

Figure 1(*b*) shows a schematic of the burner configuration examined in this work. The dual-fuel nozzle, previously characterized for Jet-A1/H_2 operation in Ref. [19], enables simultaneous delivery of liquid fuel (Jet-A1 or SAF/Jet-A1) and gaseous H_2. Both fuels are routed through a water-cooled lance to maintain near-ambient temperatures and to mitigate any coking of the liquid fuel. Jet-A1 or SAF/Jet-A1 is supplied axially using a hollow-cone atomizer (flow number 0.74, bore diameter 0.35 mm, inner half-angle 60 deg). The atomizer operates in a two-stage airblast mode: the liquid forms a thin film along the prefilmer surface, which is subsequently sheared and dispersed at the prefilmer lip by high air velocities. H_2 is introduced through 12 circumferentially distributed orifices (each 0.35 mm in diameter) positioned around the outer prefilmer. The nozzle features two main air supplies (air vanes 2 and 3) separated by a prefilmer lip. Air vanes 3 allow a non-swirled airflow on the outer side of the prefilmer, while air vanes 2 introduce swirl to the inner side of the prefilmer. In addition, a small non-

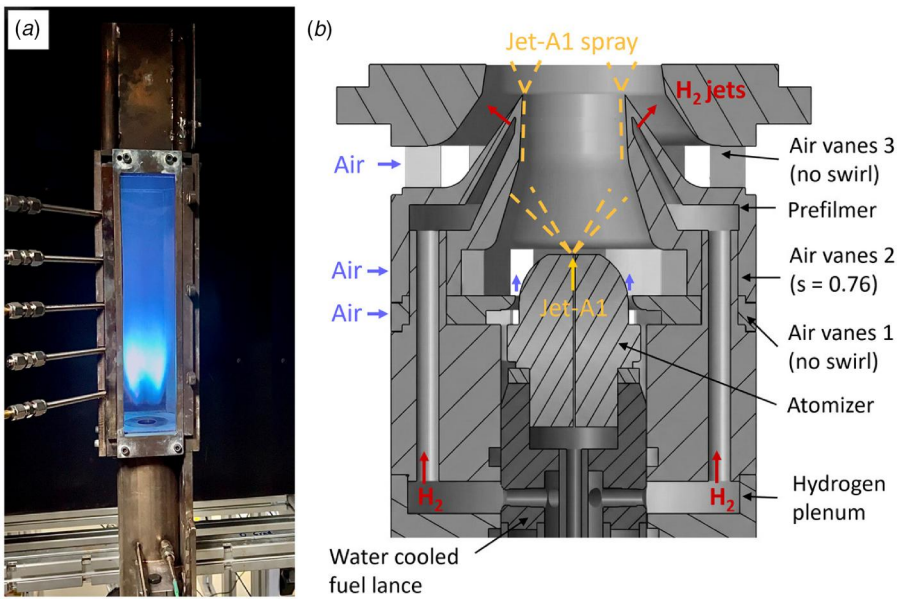


Fig. 1 (*a*) Photograph of the lab-scale gas turbine combustion chamber facility and (*b*) cross-sectional schematic of the nozzle employed in this study

Downloaded from asmedigitalcollection.asme.org/gasturbinespower/article-pdf/148/12/121009/7633651/gtp-26-1251.pdf by KIT Library user on 11 November 2026

swirling axial airflow is provided through air vanes 1 to avoid flame flashback near the burner centerline. Air vanes 2 composed of eight tangentially inclined blades whose trailing edges are oriented at 45 deg to the nozzle axis. Air vanes 1 and 3 supply non-swirling air: air vanes 1 comprise eight straight blades, while air vanes 3 contain 12 straight blades, both with zero trailing angle. The burner has an overall swirl number of approximately 0.1 (no inner recirculation zone targeted). The corresponding flow topology and mixing field under nonreacting conditions were analyzed using Reynolds-averaged Navier–Stokes simulations in our previous work [19], offering further details for interested readers.

Fuel and air flow rates are measured with high-precision instrumentation. The total combustion air flow is measured using a thermal flowmeter (Bronkhorst In-Flow, Ruurlo, The Netherlands), featuring a 0.5% of full-scale accuracy. Hydrogen flow rates are controlled by a thermal mass flow controller (Bronkhorst EL-Flow, Ruurlo, The Netherlands), offering 0.1% full-scale accuracy. Liquid fuel flow rates are measured using a Coriolis mass flowmeter (Krohne OPTIMASS 3400c, Duisburg, Germany) with an accuracy of 0.1% of full-scale accuracy.

2.2 Measurement Techniques. Side-view OH^* chemiluminescence images of the flames were captured using a high-speed camera (Phantom V1212, Wayne) coupled with a high-speed intensifier (LaVision HS-IRO, Göttingen, Germany). A 100 mm f/2.8 UV lens (Cerco, Saint-Martin-de-Crau, France) was employed together with bandpass filters (Chroma, Bellows Falls, transmission > 80% over 300–340 nm, full width at half maximum 10 nm) centered on the emission wavelength from electronically excited OH* radicals ($A^2\Sigma^+ \rightarrow X^2\Pi$). The camera was operated at 1 kHz for 10 s and recorded images at 1280 × 800 pixels. Based on the field of view of 260 mm × 160 mm, this corresponds to a spatial resolution of 203.1 μm per pixel horizontally and 200 μm per pixel vertically.

Exhaust gas measurements were obtained using a thermally regulated sampling probe, which was positioned 440 mm downstream of the burner. Gas samples were routed through a gas dehydrator to the respective analyzers under controlled pressure conditions. The concentrations of O_2 were measured with an ABB Magnos 206 sensor (Mannheim, Germany), while CO and CO_2 were determined using an ABB Uras 26 (Mannheim, Germany). Nitrogen oxides (NO_x, including NO and NO_2) were quantified with an Eco Physics CLD 700 EL (Dürnten, Switzerland) chemiluminescence detector.

2.3 Operating Conditions. The experimental campaign was first conducted to compare the baseline flames of pure Jet-A1 and SAF/Jet-A1 blend at two air inlet temperatures (T_{air}) and various specific thermal powers ($\mathcal{P}_{sp}$). In particular, the burner was operated using a SAF/Jet-A1 blend at a 40:60 volumetric ratio, with the SAF produced via the hydroprocessed esters and fatty acids process. The detailed operating conditions for experiments with pure Jet-A1 and SAF/Jet-A1 fuels are summarized in Table 1.

For dual-fuel operation with H_2, the H_2 fraction in the mixture is defined based on the relative energy contribution of each fuel under constant thermal power ($\mathcal{P}$) and fixed air mass flow rate ($\dot{m}_{air}$) [15]

$$\%H_2 = \frac{\dot{m}_{H_2} LHV_{H_2}}{\dot{m}_{H_2} LHV_{H_2} + \dot{m}_{LF} LHV_{LF}} \quad (1)$$

where LHV is the lower heating value, with $LHV_{H_2} = 119.97$ MJ/kg for H_2 and LHV_{LF} for the liquid fuels, with 43.1 MJ/kg for Jet-A1 and 48.1 MJ/kg for SAF, a volumetric blend ratio of 40:60 (SAF:Jet-A1) results in an LHV approximately 5% higher than that of pure Jet-A1. The detailed operating conditions for the fuel-flexible combustor under varying H_2 addition in Jet-A1 and SAF/Jet-A1 flames are listed in Table 2, including the corresponding T_{air} and fuel split configurations. At each T_{air}, experiments were performed in continuous operation, with H_2 content increased stepwise from the baseline liquid fuel condition. This comprehensive dataset enables a detailed analysis of flame structure, lift-off height, and pollutant emissions across a wide range of fuel blends.

3 Results and Discussion

This section presents the results, beginning with an investigation of the morphological transitions of the flame, based on OH^* chemiluminescence, at different T_{air} and $\mathcal{P}_{sp}$, with the H_2 fuel split varying from 0% to 100%. The subsequent discussion focuses on the enhancement of LBO limits and reductions in pollutant emissions achieved through H_2 addition in the low-swirl combustor.

3.1 Examination of Time-Averaged Flame Morphology. The investigation of the fuel-flexible combustor focuses on the morphological evolution of the Abel-deconvoluted OH^* chemiluminescence fields for Jet-A1 and SAF/Jet-A1 blend with varying H_2 content. The images are normalized by the highest maximum OH^* intensity of the Jet-A1 and SAF/Jet-A1 flames under each operating condition individually, facilitating a direct comparison of the flames. First, the influence of T_{air} on flame topology of liquid fuels is analyzed at two different $\mathcal{P}_{sp}$ values. This is followed by a systematic assessment of the effect of H_2 addition, ranging from 0% to 100%, on flame morphology.

3.1.1 Jet-A1 Versus Sustainable Aviation Fuel/Jet-A1 Flame Shape. Figure 2 shows time-averaged OH^* chemiluminescence images, spatially reconstructed using inverse Abel transformation, for Jet-A1 and SAF/Jet-A1 blend. In the figure, columns correspond to variations in $\mathcal{P}_{sp}$ and rows to different T_{air}, for the operating conditions listed in Table 1. Under engine-relevant conditions, the relative pressure drop across the combustor is approximately

Table 1 Operating conditions for the experiments performed with pure Jet-A1 and SAF/Jet-A1 fuels at $\Delta p/P = 3\%$

T_{air} (K)	$\dot{m}_{Jet-A1}$ (g/s)	$\dot{m}_{SAF/Jet-A1}$ (g/s)	$\dot{m}_{air}$ (g/s)	$\mathcal{P}$ (kW)	$\mathcal{P}_{sp}$ (MJ/kg$_{air}$)	U_b (m/s)
473	0.95, 0.86, 0.78, 0.69, 0.60	0	25.3	40.8, 37.1, 33.4, 29.7, 26.0	1.61, 1.46, 1.32, 1.17, 1.02	75.8
	0	0.91, 0.82, 0.74, 0.66, 0.58	25.3	40.8, 37.1, 33.4, 29.7, 26.0	1.61, 1.46, 1.32, 1.17, 1.02	75.8
673	0.79, 0.72, 0.65, 0.58, 0.51	0	21.2	34.2, 31.1, 28.0, 24.9, 21.8	1.61, 1.46, 1.32, 1.17, 1.02	90.5
	0	0.76, 0.69, 0.62, 0.55, 0.48	21.2	34.2, 31.1, 28.0, 24.9, 21.8	1.61, 1.46, 1.32, 1.17, 1.02	90.5

Table 2 Operating conditions of the fuel-flexible combustor with H_2 addition in Jet-A1 and SAF/Jet-A1 flames

T_{air} (K)	% H_2	$\dot{m}_{Jet-A1}$ (g/s)	$\dot{m}_{SAF/Jet-A1}$ (g/s)	$\dot{m}_{H_2}$ (g/s)	$\dot{m}_{air}$ (g/s)	$\mathcal{P}$ (kW)	$\mathcal{P}_{sp}$ (MJ/kg$_{air}$)	$\Delta p/P$ (%)	U_b (m/s)
473	0–100	0.86–0	0	0–0.31	25.3	37.1	1.46	3	75.8
	0–100	0	0.82–0	0–0.31	25.3	37.1	1.46	3	75.8
673	0–100	0.72–0	0	0–0.26	21.2	31.1	1.46	3	90.5
	0–100	0	0.69–0	0–0.26	21.2	31.1	1.46	3	90.5

Downloaded from asmedigitalcollection.asme.org/gasturbinespower/article-pdf/148/12/121009/7633651/gtp-26-1251.pdf by KIT Library user on 11 November 2026

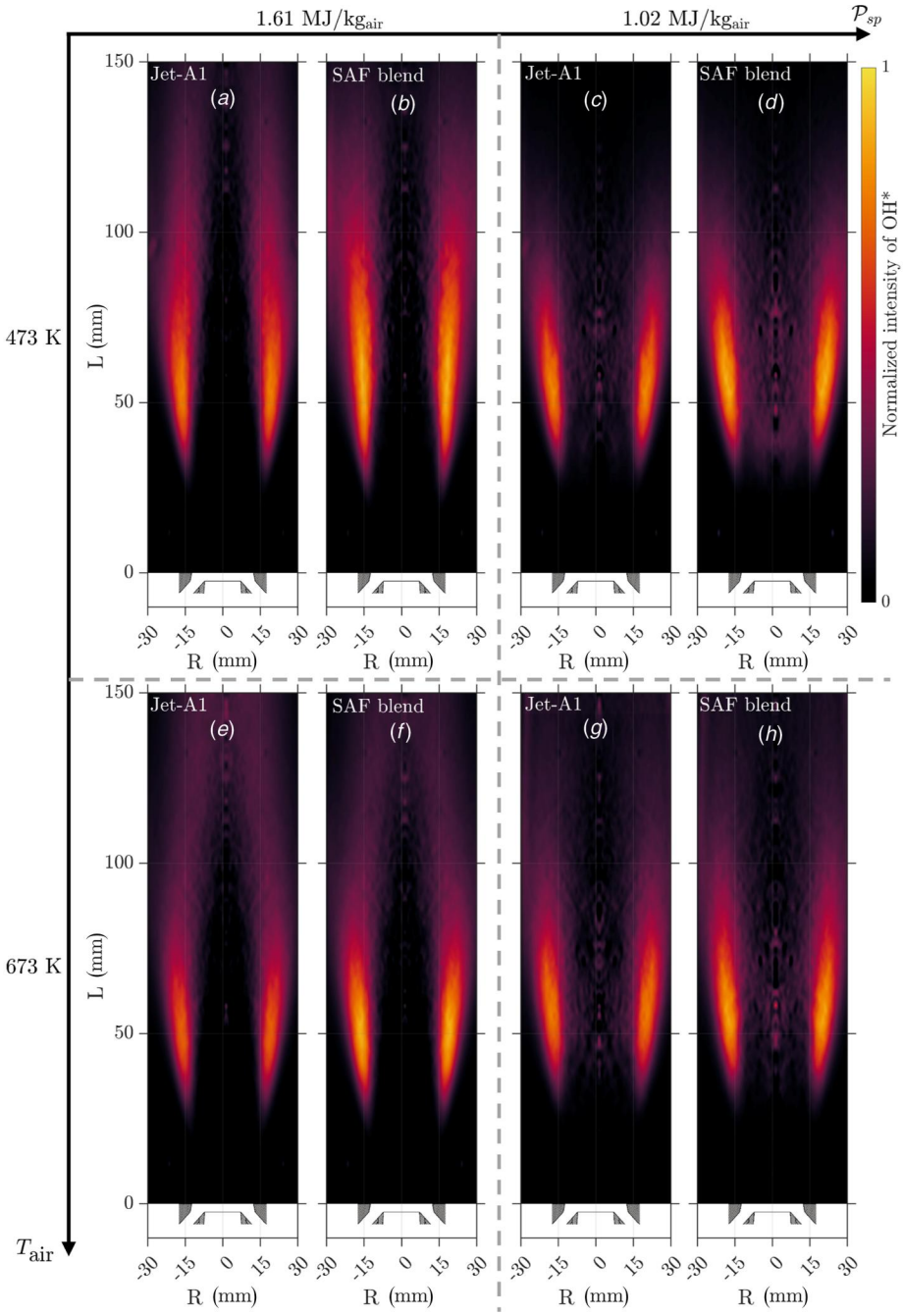


Fig. 2 Time-averaged inverse Abel-transformed OH* images of pure Jet-A1 and SAF/Jet-A1 at two specific thermal powers ($\mathcal{P}_{sp}$) and air inlet temperature of (*a*)–(*d*) T_{air}=473 K and (*e*)–(*h*) T_{air}=673 K, highlighting the influence of fuel composition on flame shape and lift-off height

invariant with T_{air}. However, the effect of the increase in bulk velocity (U_b) on the lift-off height is counterbalanced by the corresponding increase in laminar flame speed. The elevated T_{air} also promotes enhanced pre-evaporation and fuel–air premixing, leading to a more spatially uniform mixture in the combustion chamber.

Jet-A1 operation at $T_{air} = 473$ K and 673 K with $\mathcal{P}_{sp} = 1.61$ MJ/kg$_{air}$ and 1.02 MJ/kg$_{air}$ are shown in Figs. 2(*a*) and 2(*e*) and Figs. 2(*c*) and 2(*g*), while the corresponding SAF/Jet-A1 flames are shown in Figs. 2(*b*) and 2(*f*) and Figs. 2(*d*) and 2(*h*), respectively. Across all operating points, the two fuels exhibit broadly similar global flame morphology. In each case, the high-luminosity heat release zone appears spatially extended and positioned far downstream of the burner exit.

The lifted nature of the flame reflects substantial fuel pre-evaporation and premixing of fuel with air at higher T_{air}. As T_{air} increases, the lift-off height decreases slightly and the heat release zone becomes more compact, indicating stronger stabilization and more rapid heat release. This behavior is consistent with the higher laminar flame speed at elevated T_{air}. Additionally, the reduced expansion ratio between fresh and burnt gases at elevated T_{air} leads to an increase in size of the outer recirculation zone, thereby promoting earlier flame anchoring, a stabilization trend also reported by Shamma et al. [26] for Jet-A1 spray flames.

Between the two fuels, subtle but systematic differences are evident. For instance, at $T_{air} = 473$ K and $\mathcal{P}_{sp} = 1.61$ MJ/kg$_{air}$, the SAF/Jet-A1 blend (Fig. 2(*b*)) displays slightly higher OH* intensity relative to Jet-A1 (Fig. 2(*a*)), indicating marginally enhanced local

Downloaded from asmedigitalcollection.asme.org/gasturbinespower/article-pdf/148/12/121009/7633651/gtp-26-1251.pdf by KIT Library user on 11 November 2026

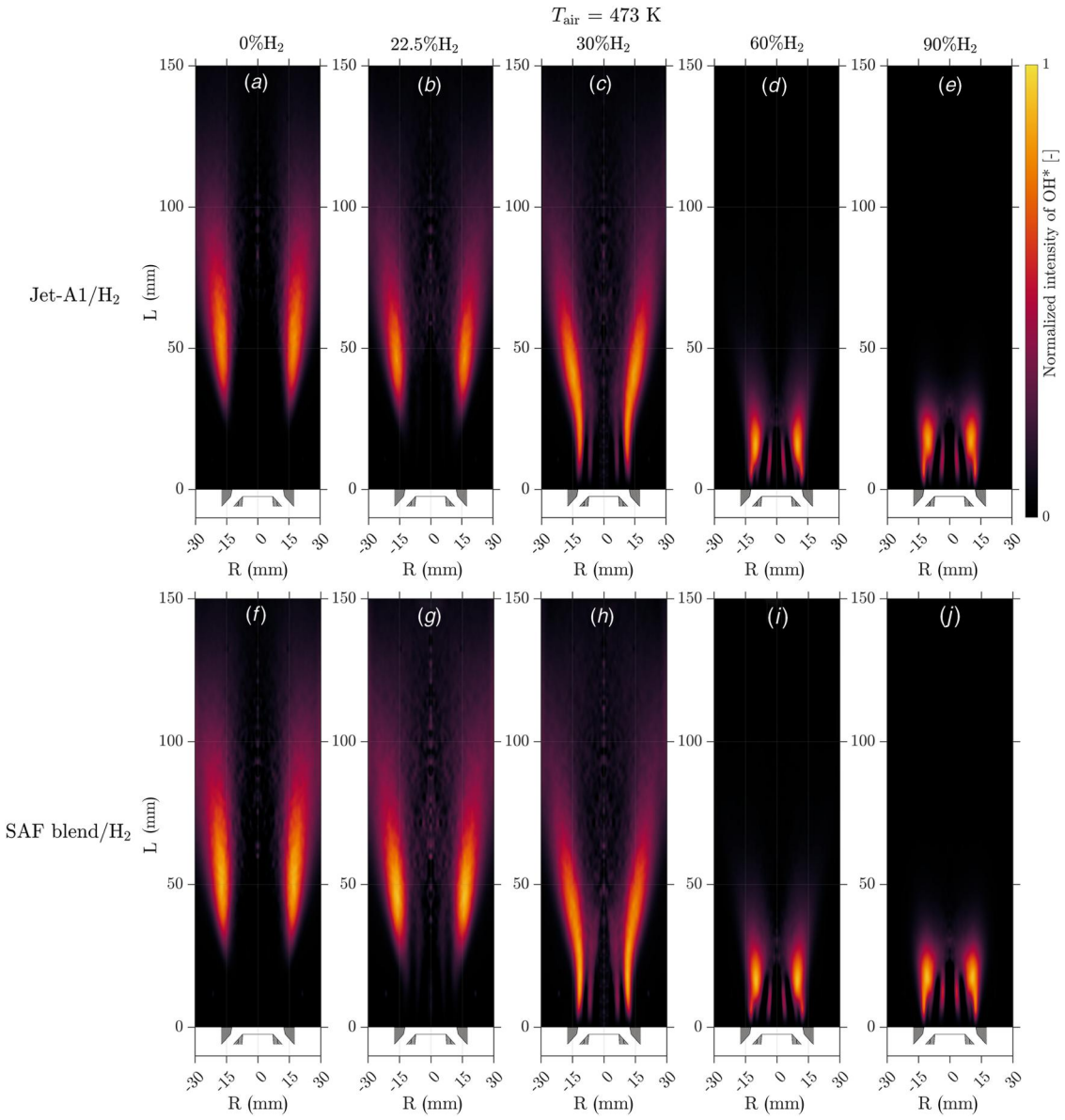


Fig. 3 Time-averaged OH* chemiluminescence images, reconstructed using inverse Abel transformation, for varying H_2 contents: (*a*)–(*e*) Jet-A1 and (*f*)–(*j*) SAF/Jet-A1 fuel splits at T_{air} = 473 K, with constant $\mathcal{P}_{sp}$ = 1.46 MJ/kg$_{air}$ and $\Delta p/P$ = 3%

heat release and reaction rates. The SAF/Jet-A1 flame also appears longer, with a moderately lower LOH, defined here as the axial distance between the nozzle exit and the flame base, and a narrower lateral spread compared to Jet-A1. At elevated $T_{air} = 673$ K and the same $\mathcal{P}_{sp}$, the SAF/Jet-A1 blend (Fig. 2(*f*)) again shows higher OH* intensity relative to Jet-A1 (Fig. 2(*e*)). However, the global flame structure of the two fuels becomes more similar under these conditions, although the SAF/Jet-A1 flame retains a slightly higher LOH. A potential reason could be differences between the two fuels in their atomization performance and evaporation characteristics. At lower T_{air}, slower droplet evaporation makes flame stabilization more sensitive to fuel-dependent spray and evaporation characteristics, leading to larger differences in lift-off height and flame shape. At higher T_{air}, rapid droplet evaporation near the nozzle reduces the influence of spray effects, with remaining differences in flame structure primarily governed by fuel composition.

At the lower $\mathcal{P}_{sp}$, the global flame morphology of the two fuels becomes nearly indistinguishable across both $T_{air} = 473$ K and 673 K, with the SAF/Jet-A1 blend showing only a modest, but still discernible, increase in OH* intensity relative to Jet-A1. For intermediate $\mathcal{P}_{sp}$, the LOH difference between the SAF/Jet-A1 and Jet-A1 flames decreases with decreasing $\mathcal{P}_{sp}$, with the largest difference at the highest and the smallest at the lowest specific thermal power. Across all operating conditions, the OH* intensity remains consistently higher for the SAF/Jet-A1 flame than for the Jet-A1 flame.

3.1.2 Impact of H_2 Addition on Flame Shape. In aero-engine operation, adjusting the H_2 fuel split will be essential for optimizing performance and emissions while maintaining constant thermal power, particularly during high-demand conditions such as takeoff operation [15,27]. In Figs. 3 and 4, a specific thermal power of $\mathcal{P}_{sp} = 1.46$ MJ/kg$_{air}$ was chosen, corresponding to an equivalence ratio of $\approx$0.5 for Jet-A1 combustion, representative of maximum thrust operating conditions in aero-engines. Figure 3 shows time-averaged inverse Abel-transformed OH* images for varying H_2 contents at $T_{air} = 473$ K, with constant $\mathcal{P}_{sp} = 1.46$ MJ/kg$_{air}$ and relative pressure drop of 3% (see Table 2). The top and bottom rows correspond to Jet-A1 and SAF/Jet-A1, respectively.

For pure Jet-A1 and SAF/Jet-A1 operation (Figs. 3(*a*) and 3(*f*)), the high-luminosity heat release zone is broad and positioned far downstream of the fuel nozzle. SAF/Jet-A1 consistently exhibits a

Downloaded from asmedigitalcollection.asme.org/gasturbinespower/article-pdf/148/12/121009/7633651/gtp-26-1251.pdf by KIT Library user on 11 November 2026

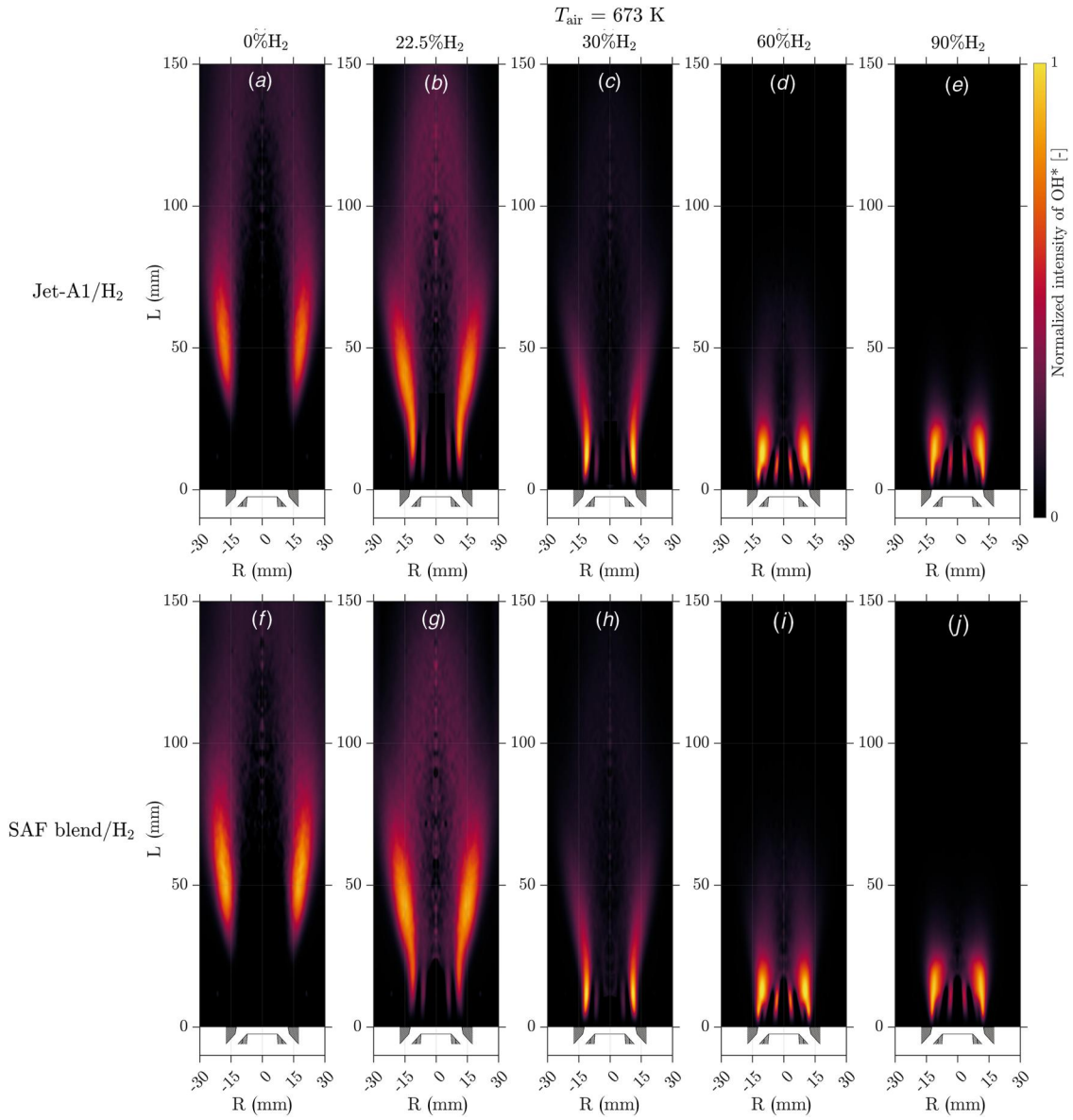


Fig. 4 Time-averaged OH* chemiluminescence images, reconstructed using inverse Abel transformation, for varying H_2 contents: (*a*)–(*e*) Jet-A1 and (*f*)–(*j*) SAF/Jet-A1 fuel splits at T_{air}=673 K, with constant $\mathcal{P}_{sp}$ = 1.46 MJ/kg_{air} and $\Delta p/P$ = 3%

slightly lower LOH and a more intense heat release zone compared with Jet-A1, indicating enhanced reactivity due to its altered physical and chemical properties. Up to 22.5% H_2 addition (Figs. 3(*b*) and 3(*g*)), the overall flame shape remains similar to the baseline liquid-fuel flames, with only a modest reduction in LOH. This behavior reflects the increased flame speed from H_2 combined with limited radial penetration of the H_2 jets, which allows the Jet-A1 or SAF/Jet-A1 combustion mode to remain dominant. Correspondingly, SAF/Jet-A1 flame continues to exhibit a slightly stronger heat release intensity and a marginally shorter LOH than Jet-A1. As the H_2 content increases to 30% (Figs. 3(*c*) and 3(*h*)), the flame becomes more compact and shifts noticeably toward the burner exit. This upstream stabilization arises from the higher reactivity of the mixture and from stronger radial H_2 penetration, which enriches the outer recirculation zone and enhances anchoring near the nozzle. For the SAF/Jet-A1 flame, the luminous heat release zone also extends closer to the burner exit compared with Jet-A1, consistent with its intensified heat release zone.

Beyond 30% and up to 100% H_2 fuel split, H_2 governs the flame stabilization mechanism. The remaining Jet-A1 or SAF/Jet-A1 contributes only to an extended downstream release zone, and its influence diminishes steadily as its fraction decreases. As a result, both fuel blends (liquid fuel with H_2) converge toward nearly identical flame structures under H_2-rich conditions. For instance, at 60% H_2 (Figs. 3(*d*) and 3(*i*)), the dominant heat release zone shifts further upstream, approaching the burner exit. For further higher H_2 blends, the flame exhibits a highly compact heat release zone, positioned near the burner exit yet remaining distinctly detached from the burner, as illustrated for 90% H_2 in Figs. 3(*e*) and 3(*j*). Operation at 100% H_2 shows a flame structure similar to that at 90% H_2 and is reported separately in Ref. [19].

Figure 4 shows time-averaged images for varying H_2 contents at T_{air} = 673 K and $\mathcal{P}_{sp}$ = 1.46 MJ/kg_{air}, with the top and bottom rows corresponding to Jet-A1 and SAF/Jet-A1, respectively. The operating conditions for each fuel split are identical to those shown in Fig. 3 and summarized in Table 2. The higher laminar flame speed leads to a slight reduction in LOH at elevated T_{air} (Figs. 4(*a*) and 4(*f*)). Both pure Jet-A1 and pure SAF/Jet-A1 flames exhibit significantly more compact heat release zones than those observed at 473 K (Figs. 3(*a*) and 3(*f*)). Consistent with earlier observations,

Downloaded from asmedigitalcollection.asme.org/gasturbinespower/article-pdf/148/12/121009/7633651/gtp-26-1251.pdf by KIT Library user on 11 November 2026

SAF/Jet-A1 again exhibits a slightly lower LOH and a more intense heat release zone.

For H_2 additions up to 15% (not shown for brevity), the flame structure remains largely similar to the baseline liquid-fuel cases, with only modest reductions in LOH. However, the upstream shift of the heat release zone with increasing H_2 is notably more pronounced at 673 K than at 473 K. For instance, at 22.5% H_2 (Figs. 4(*b*) and 4(*g*)), the high-luminosity heat release zone shifts closer to the burner exit and becomes elongated, in contrast to Figs. 3(*b*) and 3(*g*), where the flames remain farther downstream. This behavior arises primarily from the substantially higher flame speed of H_2 at elevated T_{air}. At 30% H_2 (Figs. 4(*c*) and 4(*h*)), the heat release zone shifts further upstream and becomes more compact compared to Figs. 3(*c*) and 3(*h*), reflecting stronger H_2-dominated stabilization. The remaining Jet-A1 and SAF/Jet-A1 contribute only to an extended downstream heat release zone. Beyond 30% H_2 blends, a highly compact heat release zone is observed in Figs. 4(*d*), 4(*e*), 4(*i*), and 4(*j*). Although increasing the H_2 content beyond 30% degrades the overall premixing quality and can generate near-stoichiometric pockets at large radii near the nozzle periphery, the axial position of the high-luminosity heat release zone remains essentially unchanged. This invariance likely reflects the burner geometry, which provides a uniformly distributed, high-velocity airflow field at the exit. Additionally, the orientation of the H_2 jets increases the axial momentum component as the H_2 fuel split rises, keeping the flame detached despite its proximity to the burner.

3.2 Flame Lift-Off Height for Fuel-Flexible Combustor. The LOH is a key parameter, as it governs the extent of fuel–air mixing prior to combustion and provides an important indicator of pollutant emission behavior. In this study, LOH is defined as the axial distance between the fuel nozzle exit and the base of the flame. The measurement was obtained from OH^* chemiluminescence imaging, where LOH corresponds to the distance from the nozzle exit to the horizontal location upstream of which only 5% of the total integrated OH^* intensity is detected. This relatively threshold was deliberately selected to reduce the influence of variations in OH^* signal strength arising from differences between Jet-A1 and SAF/Jet-A1 flames, as well as from the systematic addition of H_2, thereby ensuring consistency and comparability across all operating conditions.

Figure 5 shows the variation of LOH with increasing H_2 content for Jet-A1 and SAF/Jet-A1 flames at the two investigated T_{air} conditions. At 473 K, the pure SAF/Jet-A1 flame exhibits a slightly lower LOH than the pure Jet-A1 flame, whereas at 673 K, the LOH values are low and nearly identical for both fuels. As discussed earlier, this behavior may correspond to slight differences in the atomization and evaporation of SAF/Jet-A1, which play a significant role at lower T_{air}. As the H_2 content increases, the LOH decreases markedly for both T_{air}. For lower T_{air}, the reduction in LOH remains modest up to approximately 22.5% H_2, while at higher T_{air} LOH remains modest up to 15% H_2. This behavior is likely due to an increased flame speed by H_2 addition in combination with a low radial H_2 jet penetration, which maintains Jet-A1 or SAF/Jet-A1 combustion as the dominant process in this regime. At 30% H_2, the flame begins to stabilize within the outer recirculation zone near the burner exit for both T_{air} conditions. This shift in anchoring location arises from the stronger radial penetration of the H_2 jets, which promote the formation of a locally fuel-rich mixture near the outer recirculation region (see Figs. 3(*c*), 3(*h*), 4(*c*), and 4(*h*)). A small but noticeable distinction between SAF/Jet-A1 and Jet-A1 persists up to approximately 37.5% H_2, beyond which the LOH values converge for low T_{air} and remain nearly identical at high T_{air} for all the fuel splits. Alternatively, the observed reduction in LOH with increasing H_2 fuel split can be interpreted in terms of the jet-to-crossflow momentum flux ratio (J). The parameter J is defined as the ratio of the H_2 jet to freestream air momentum fluxes: $J = \rho_{H_2} u_{H_2}^2 / \rho_{air} U_{air}^2$ [28], where ρ and U denote the density and velocity of the respective flows. Under the present conditions, J increases from approximately 3.3 to 20.5 at $T_{air} = 473$ K and from 2.3 to 14.4 at $T_{air} = 673$ K as the H_2 fuel split increases from 15% to 37.5%. At low J, the H_2 jet is insufficient to significantly affect the flame, whereas higher J promotes higher radial jet penetration and mixing, thereby reducing LOH. At further higher fuel splits, the increasingly fuel-rich mixture near the burner periphery further reduces the calculated LOH, leading to a more compact anchored flame (see Figs. 3(*e*), 3(*j*), 4(*e*), and 4(*j*)).

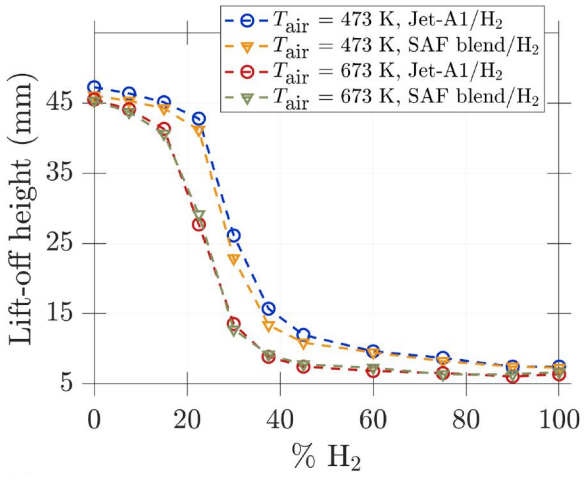


Fig. 5 Variation of flame lift-off height as a function of H_2 blending for different T_{air} in Jet-A1 and SAF/Jet-A1 operations, with the corresponding operating conditions listed in Table 2

3.3 Flame Width Variation With H_2 Addition. The flame width is another key parameter extracted from the time-averaged Abel-transformed OH^* chemiluminescence fields for the quantitative characterization of differences between Jet-A1 and SAF/Jet-A1 flames. The flame width is defined as the maximum radial extent of the OH^* intensity distribution corresponding to a normalized intensity threshold of 50%, representing the full width at half maximum of the heat release zone [29]. The maximum radial flame spread corresponds to the largest lateral distance between the left and right flame edges over the entire axial length of the flame. This parameter complements the axial stabilization information obtained from LOH and enables an objective comparison of flame morphology across fuel types and operating conditions.

Figure 6 shows the variation of flame width with increasing H_2 content for Jet-A1 and SAF/Jet-A1 flames at the two investigated T_{air} conditions. At $T_{air} = 473$ K, the pure SAF/Jet-A1 flame exhibits a slightly smaller flame width than the pure Jet-A1 flame. At $T_{air} = 673$ K, the flame widths are generally lower than those at 473 K and nearly identical for both fuels, indicating a diminished influence of spray effects at elevated T_{air}.

With increasing H_2 content, the flame width decreases systematically for both T_{air} conditions. At 473 K, the flame width decreases gradually and remains relatively modest up to approximately 30% H_2, whereas at 673 K, it remains modest only up to about 22.5% H_2, followed by a pronounced reduction at higher H_2 fuel splits. In particular, between 30% and 60% H_2, the flame width remains consistently low compared to lower fuel splits, reflecting the enhanced flame speed and reactivity associated with H_2 addition. This results in faster fuel consumption and a more compact reaction zone, which limits radial flame expansion. Notably, a small but noticeable distinction between SAF/Jet-A1 and Jet-A1 persists up to approximately 37.5% H_2; beyond this point, the flame width values converge for low T_{air} and remain nearly identical at high T_{air} for all the fuel splits. Beyond 60% H_2, the flame width increases systematically, likely due to higher volumetric fuel flow near the burner exit and the stronger momentum of the H_2 jets.

3.4 Lean Blowout Limit Improvements. Operating a combustor at low thermal power inherently increases its susceptibility to

Downloaded from asmedigitalcollection.asme.org/gasturbinespower/article-pdf/148/12/121009/7633651/gtp-26-1251.pdf by KIT Library user on 11 November 2026

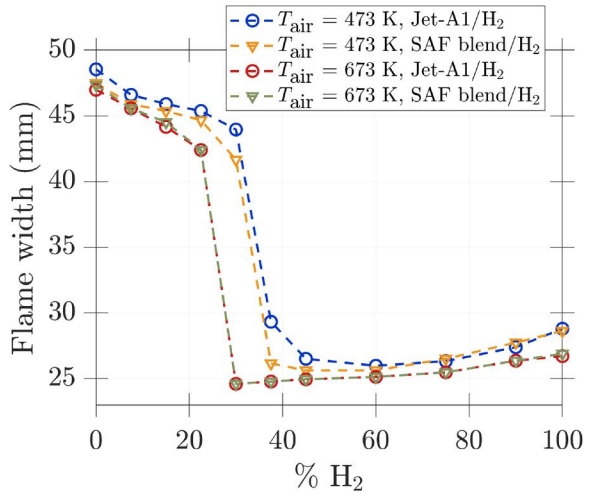


Fig. 6 Variation of flame width as a function of H_2 blending for different T_{air} in Jet-A1 and SAF/Jet-A1 operations, with the corresponding operating conditions listed in Table 2

LBO, as the reduced heat release and slower reaction rates are often insufficient to sustain a stable flame. The impact of fuel composition on the blowout limit is therefore of critical importance in the design of lean combustion systems. As the fuel–air mixture becomes excessively lean, local extinction driven by high strain rates and reduced reaction-zone robustness can destabilize the flame and ultimately lead to global blowout. The LBO limit, commonly defined as the maximum air-to-fuel ratio or minimum thermal power at which a flame can be sustained before extinction, determines the minimum fuel flow required for stable operation under specific conditions. Incorporating H_2 into Jet-A1 or SAF/Jet-A1 spray flames offers a promising approach to reconcile the competing demands of ultralean operation, flame stability, and emissions reduction. In this context, the present study investigates the influence of H_2 addition on the LBO characteristics of a fuel-flexible low-swirl combustor.

Figure 7 shows the LBO limits for Jet-A1 and SAF/Jet-A1 flames with varying H_2 additions at two T_{air} conditions, measured at a constant bulk velocity U_b (see Table 2). The LBO thermal power ($\mathcal{P}_{LBO}$) is determined by gradually reducing the thermal power until global flame extinction occurs. For the LBO experiments, each fuel

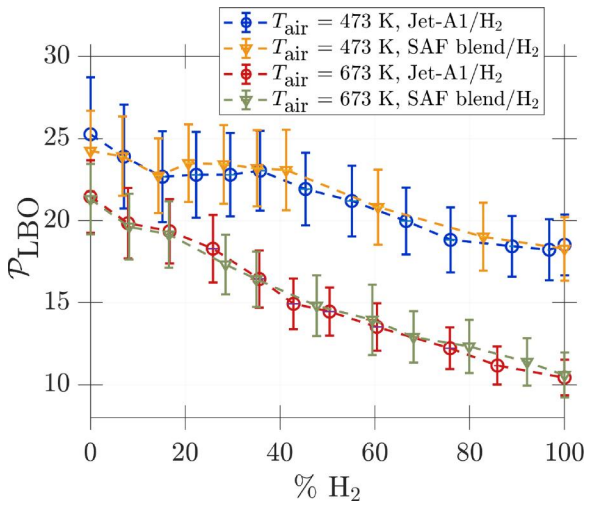


Fig. 7 LBO limits for varying H_2 blends in Jet-A1 and SAF/Jet-A1 operations. Operating conditions are in Table 2, and error bars denote the combined measurement uncertainty (coverage factor of 2), incorporating both statistical and systematic contributions.

split was investigated individually: the H_2 flow rate ($\dot{m}_{H_2}$) was maintained constant within the selected range, while the liquid fuel flow rate was gradually reduced until flame extinction occurred. Error bars represent the combined uncertainty (coverage factor of 2) at each fuel split, accounting for both statistical variability from three repeated measurements and systematic uncertainties. Within the uncertainty bounds, the decrease in $\mathcal{P}_{LBO}$ with increasing H_2 content is clearly resolved. The separation between the liquid fuels (Jet-A1 and SAF/Jet-A1) and their H_2 addition blends is unambiguous across both T_{air} conditions. At 473 K, $\mathcal{P}_{LBO}$ decreases from 25.3 kW (pure Jet-A1) and 24.25 kW (pure SAF/Jet-A1) to 18.3 kW (pure H_2). This reduction is more pronounced at higher T_{air}, with $\mathcal{P}_{LBO}$ dropping from 21.3 kW to 10.6 kW between pure Jet-A1 and SAF/Jet-A1 to pure H_2. These results show that even modest H_2 addition significantly lowers the LBO limit, enhancing flame stability and extending the operable range in aero-engines, both at high T_{air} during takeoff/climb, and at lower T_{air} relevant for idle/taxiing conditions.

Particularly, pure Jet-A1 and SAF/Jet-A1 flames exhibit higher $\mathcal{P}_{LBO}$ at both T_{air} compared to pure H_2, consistent with the lower reactivity and slower burning velocities of hydrocarbon flames. Jet-A1 and SAF/Jet-A1 flames show nearly identical LBO limits at both T_{air} conditions. For H_2 content up to 30%, the influence of H_2 on $\mathcal{P}_{LBO}$ remains relatively consistent across both T_{air}. This behavior likely reflects limited H_2 jet penetration and the continued dominance of the liquid-fuel spray in controlling the flame stabilization mechanism.

Notably, the LBO limits for Jet-A1 and SAF/Jet-A1 with H_2 addition remain closely aligned across the two T_{air}, reinforcing the suitability of SAF/Jet-A1 as a drop-in replacement for Jet-A1 fuel. For H_2 contents between 30% and 100%, $\mathcal{P}_{LBO}$ decreases progressively with increasing H_2 contents for both fuels. This improvement in stability arises from the enhanced reaction rates, higher diffusivity, and increased burning velocity of H_2-enriched flames. In this regime, a clear divergence between the two T_{air} cases becomes evident, with higher T_{air} demonstrating substantially lower LBO limits, especially for close to 100% H_2 operations. Overall, H_2 addition markedly enhances flame stability by reducing the required $\mathcal{P}$ for sustained combustion and expanding the operating margin against blowout. These results highlight the potential of H_2 to extend the stable operating range of fuel-flexible combustors while accommodating both Jet-A1 and SAF blend.

3.5 Pollutant Emissions Measurements. NO_x and CO emissions are key considerations in the development of gas turbine combustors. First, the dry exhaust gases (NO_x and CO emissions) for pure Jet-A1 and SAF/Jet-A1 fuels at various $\mathcal{P}_{sp}$ and two different T_{air} are examined. Next, the emissions of the fuel-flexible combustor are shown for different H_2 fuel split (0–100%). All NO_x and CO concentrations are reported in ppm and normalized by 15% O_2.

3.5.1 Emissions From Jet-A1 and Sustainable Aviation Fuel/Jet-A1 Flames. Figure 8 illustrates the NO_x and CO emissions for pure Jet-A1 and SAF/Jet-A1 fuels at various $\mathcal{P}_{sp}$, under the conditions listed in Table 1. As shown in Fig. 8(*a*), NO_x levels increase with $\mathcal{P}_{sp}$ for both T_{air}; however, emissions remain relatively low due to the lifted flame. In contrast, Fig. 8(*b*) shows that CO emissions decrease with $\mathcal{P}_{sp}$, indicating more complete combustion at higher $\mathcal{P}_{sp}$. At elevated T_{air}, enhanced fuel pre-evaporation and improved mixing promote greater fuel–air homogeneity, reducing overall NO_x and CO emissions.

However, the NO_x emissions are slightly higher and CO emissions slightly lower from SAF/Jet-A1 fuel compared to Jet-A1 across all $\mathcal{P}_{sp}$ and both T_{air}. Consequently, as indicated by the averaged OH^* images (Figs. 3 and 4), the flame exhibits higher local temperatures, leading to increased NO_x emissions, while enhanced combustion reduces CO emissions. Moreover, the very low and nearly identical CO emissions observed at T_{air} of 673 K can be attributed to more complete combustion across all $\mathcal{P}_{sp}$. At such T_{air}, fuel evaporation and associated air–fuel mixing are significantly

Downloaded from asmedigitalcollection.asme.org/gasturbinespower/article-pdf/148/12/121009/7633651/gtp-26-1251.pdf by KIT Library user on 11 November 2026

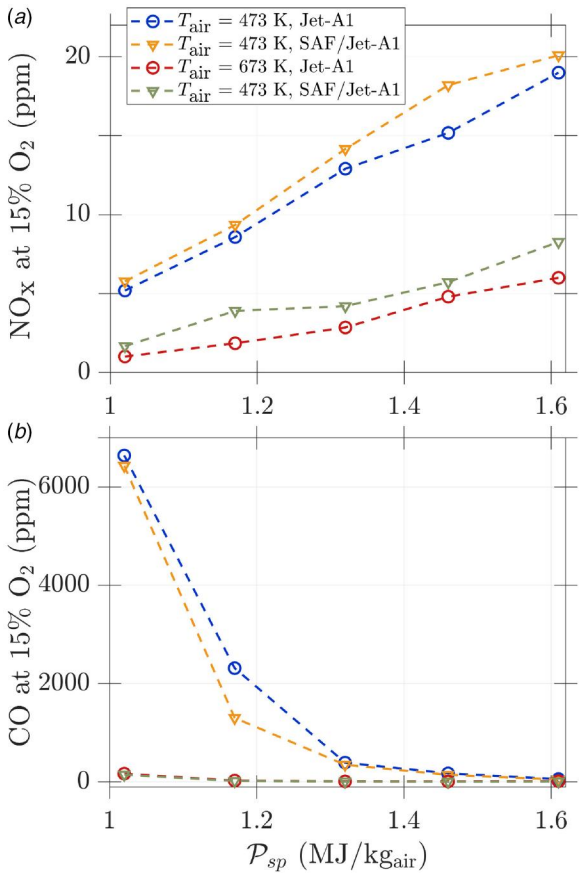


Fig. 8 Variation of NO_x and CO emissions with specific thermal power ($\mathcal{P}_{sp}$) for Jet-A1 and SAF/Jet-A1 fuels. The operating conditions are listed in Table 1.

enhanced, minimizing differences in CO formation between the Jet-A1 and SAF/Jet-A1 flames.

3.5.2 Effect of H_2 Addition on Emissions. Next, the effect of H_2 addition on pollutant emissions for Jet-A1 and SAF/Jet-A1 flames is examined. Figure 9 presents the NO_x and CO concentrations for various H_2 fuel splits, under the operating conditions listed in Table 2. Figure 9(*a*) illustrates the impact of H_2 blends on NO_x emissions at different T_{air}. For pure Jet-A1, NO_x concentrations remain lower than in the pure H_2 case, most likely because the lifted flame promotes enhanced premixing, therefore, lower peak temperatures. For pure SAF/Jet-A1, NO_x levels are comparable to those of pure H_2 at 473 K. Increasing T_{air} to 673 K accelerates fuel pre-evaporation and improves premixing for both Jet-A1 and SAF/Jet-A1, enhancing fuel–air homogeneity and reducing overall NO_x formation. At low T_{air}, NO_x emissions initially decrease with H_2 addition up to 45%, whereas at high T_{air}, NO_x emissions increase due to higher adiabatic flame temperatures. Notably, NO_x levels are slightly higher for SAF/Jet-A1 than for Jet-A1, with the largest difference at 0% H_2, gradually converging toward 45% H_2, and remaining similar at higher fuel splits. Beyond 45% H_2, the local fuel–air mixture becomes richer as the high-velocity H_2 jet penetrates radially toward the nozzle periphery, leading to locally elevated flame temperatures and increased NO_x emissions. For pure H_2 flames, the significant rise in NO_x at high T_{air} compared to low T_{air} arises from the combination of higher adiabatic flame temperatures and less effective mixing, since the nozzle geometry is optimized for H_2 fuel splits up to 30%. Consistent with this design intent, nonreacting mixing-field analyses show that, for H_2 contents up to 30%, no burnable mixture reaches the burner periphery [19].

Figure 9(*b*) shows that CO emissions decrease with increasing H_2 content in the fuel blend for both Jet-A1 and SAF/Jet-A1. For pure Jet-A1, CO emissions reach a maximum of 179 ppm at $T_{air} = 473$ K and 11.7 ppm at $T_{air} = 673$ K, while for pure SAF/Jet-A1, the maxima are 146.8 ppm at 473 K and 9.9 ppm at 673 K. Notably, even a modest H_2 addition of 15% significantly reduces CO emissions to 55.4 ppm for Jet-A1 and 43.5 ppm for SAF/Jet-A1 at the lower T_{air} of 473 K. This reduction is particularly relevant under low-thrust conditions in aero-engines, such as idle and taxiing. Beyond 45% H_2, CO emission levels for both fuel blends become nearly identical across both air inlet temperatures, and at very high H_2 contents, CO emissions approach near-zero values. This indicates that at elevated T_{air} and high H_2 fuel splits, CO emissions become largely insensitive to fuel composition under the examined operating conditions.

4 Conclusion

The current study demonstrates the successful operation of a novel low-swirl dual-fuel combustor capable of handling the full spectrum of fuel blends, from pure Jet-A1 and SAF/Jet-A1 to pure H_2. This combustor utilizes a lean-lifted spray flame concept augmented with circumferentially arranged hydrogen injectors in a jet in crossflow configuration. The combined approach enables stable, fuel-flexible operation over a wide range of thermal powers, H_2 fuel splits, and elevated air inlet temperatures.

Systematic characterization of flame morphology reveals that pure SAF/Jet-A1 generally exhibits modestly higher OH^* intensity, lower lift-off heights, and longer flame lengths than Jet-A1 at elevated inlet temperatures, especially under higher thermal loads. These distinctions diminish at lower thermal powers. When H_2 is introduced, it consistently shifts flame stabilization upstream, markedly reducing lift-off height for both liquid fuel operations. Additionally, the flame width decreases gradually at low H_2 blends and contracts sharply at higher H_2 blends. Differences between the Jet-A1 and SAF/Jet-A1 flame structures persist only at low air inlet temperatures and low H_2 content, becoming negligible at higher blends. Moreover, H_2 addition also provides a substantial

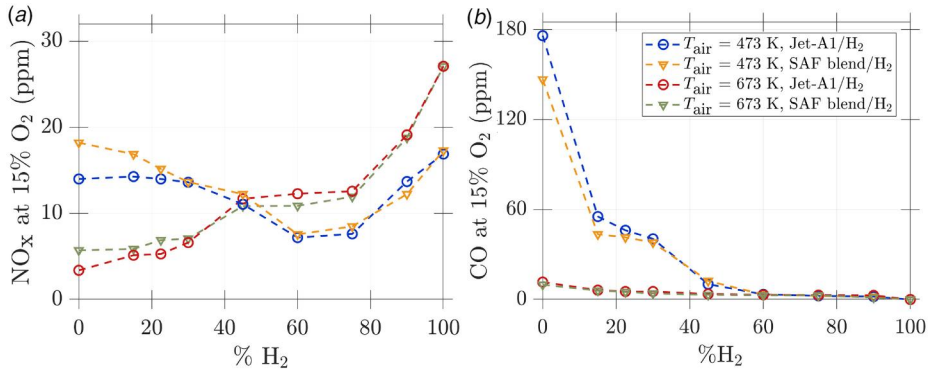


Fig. 9 Variation of NO_x and CO emissions with H_2 addition in Jet-A1 and SAF/Jet-A1 operations. The operating conditions are listed in Table 2.

Downloaded from asmedigitalcollection.asme.org/gasturbinespower/article-pdf/148/12/121009/7633651/gtp-26-1251.pdf by KIT Library user on 11 November 2026

enhancement in LBO performance. While low H_2 fuel splits offer modest improvements, higher H_2 blends nearly double the LBO limits at elevated air inlet temperature.

Up to 45% H_2 fuel splits, NO_x emissions decrease at 473 K and increase at 673 K with an increase in H_2 content. In particular, SAF/Jet-A1 initially exhibits slightly higher NO_x emissions than Jet-A1, but these differences diminish progressively with increasing H_2 content and become negligible beyond 45%. Between 45% and 75% H_2, NO_x emissions remain roughly around 10 ppm, rising significantly only at higher blends. These observations indicate that the favorable emissions performance of the fuel-flexible combustor is maintained only up to a certain H_2 threshold. Importantly, even a modest H_2 addition in the combustor, around 15%, produces a marked reduction in CO emissions at low air inlet temperatures, a benefit particularly relevant for low-thrust aero-engine operation.

Overall, Jet-A1 and SAF/Jet-A1 exhibit similar responses to H_2 addition, with only minor deviations at low H_2 blends and low air inlet temperature. The results affirm that the SAF/Jet-A1 blend in a 40:60 volumetric ratio functions effectively as a drop-in fuel in a fuel-flexible combustor. This work provides critical insights into flame dynamics, combustor stability, and emissions performance, supporting the development of next-generation aero-engines engineered to operate cleanly and reliably across a wide spectrum of sustainable and alternative fuels.

Acknowledgment

The research leading to these results has received funding from the European Union (Project: FFLECS; Grant Agreement No. 101096436). Views and opinions expressed are however those of the authors only and do not necessarily reflect those of the European Union. Neither the European Union nor the granting authority can be held responsible for them.

Conflict of Interest

There are no conflicts of interest.

Funding Data

- European Union (Project: FFLECS; Grant Agreement No. 101096436).

Data Availability Statement

The data and information that support the findings of this article are freely available at[2].

Nomenclature

CO = carbon oxide
CO_2 = carbon dioxide
H_2 = hydrogen
J = momentum flux ratio
LBO = lean blowout
LOH = lift-off height
NO_x = includes NO, NO_2
O_2 = dioxygen
$\mathcal{P}$ = thermal power
$\mathcal{P}_{sp}$ = specific thermal power
SAF = sustainable aviation fuel
T_{air} = air preheating temperature
U_b = bulk velocity
ϕ = equivalence ratio

References

[1] Gutiérrez-Antonio, C., Gómez-Castro, F. I., de Lira-Flores, J. A., and Hernández, S., 2017, "A Review on the Production Processes of Renewable Jet Fuel," Renewable Sustainable Energy Rev., **79**, pp. 709–729.
[2] Lim, J. H. K., Gan, Y. Y., Ong, H. C., Lau, B. F., Chen, W.-H., Chong, C. T., Ling, T. C., and Klemeš, J. J., 2021, "Utilization of Microalgae for Bio-Jet Fuel Production in the Aviation Sector: Challenges and Perspective," Renewable Sustainable Energy Rev., **149**, p. 111396.
[3] Shahabuddin, M., Alam, M. T., Krishna, B. B., Bhaskar, T., and Perkins, G., 2020, "A Review on the Production of Renewable Aviation Fuels From the Gasification of Biomass and Residual Wastes," Bioresour. Technol., **312**, p. 123596.
[4] Abrantes, I., Ferreira, A. F., Silva, A., and Costa, M., 2021, "Sustainable Aviation Fuels and Imminent Technologies—CO_2 Emissions Evolution Towards 2050," J. Cleaner Prod., **313**, p. 127937.
[5] Boretti, A., 2024, "Towards Hydrogen Gas Turbine Engines Aviation: A Review of Production, Infrastructure, Storage, Aircraft Design and Combustion Technologies," Int. J. Hydrogen Energy, **88**, pp. 279–288.
[6] Wang, B., Ting, Z. J., and Zhao, M., 2024, "Sustainable Aviation Fuels: Key Opportunities and Challenges in Lowering Carbon Emissions for Aviation Industry," Carbon Capture Sci. Technol., **13**, p. 100263.
[7] Yang, F., and Yao, Y., 2025, "Sustainable Aviation Fuel Pathways: Emissions, Costs and Uncertainty," Resour., Conserv. Recycl., **215**, p. 108124.
[8] Bicer, Y., and Dincer, I., 2017, "Life Cycle Evaluation of Hydrogen and Other Potential Fuels for Aircrafts," Int. J. Hydrogen Energy, **42**(16), pp. 10722–10738.
[9] Najjar, Y. S., 2013, "Hydrogen Safety: The Road Toward Green Technology," Int. J. Hydrogen Energy, **38**(25), pp. 10716–10728.
[10] Bhuiyan, M. M. H., and Siddique, Z., 2025, "Hydrogen as an Alternative Fuel: A Comprehensive Review of Challenges and Opportunities in Production, Storage, and Transportation," Int. J. Hydrogen Energy, **102**, pp. 1026–1044.
[11] Manigandan, S., Praveenkumar, T., Ryu, J. I., Verma, T. N., and Pugazhendhi, A., 2023, "Role of Hydrogen on Aviation Sector: A Review on Hydrogen Storage, Fuel Flexibility, Flame Stability, and Emissions Reduction on Gas Turbines Engines," Fuel, **352**, p. 129064.
[12] Brodzik, Ł., Prokopowicz, W., Ciupek, B., and Frąckowiak, A., 2025, "Minimizing the Environmental Impact of Aircraft Engines With the Use of Sustainable Aviation Fuel (SAF) and Hydrogen," Energies, **18**(3), p. 472.
[13] Hiroyasu, H., Arai, M., Kadota, T., and Yoso, J., 1980, "An Experimental Study on Kerosene-Hydrogen Hybrid Combustion in a Gas Turbine Combustor," Bull. JSME, **23**(184), pp. 1655–1662.
[14] Juste, G., 2006, "Hydrogen Injection as Additional Fuel in Gas Turbine Combustor. Evaluation of Effects," Int. J. Hydrogen Energy, **31**(14), pp. 2112–2121.
[15] Frenillot, J., Cabot, G., Cazalens, M., Renou, B., and Boukhalfa, M., 2009, "Impact of H_2 Addition on Flame Stability and Pollutant Emissions for an Atmospheric Kerosene/Air Swirled Flame of Laboratory Scaled Gas Turbine," Int. J. Hydrogen Energy, **34**(9), pp. 3930–3944.
[16] Burguburu, J., Cabot, G., Renou, B., Boukhalfa, A. M., and Cazalens, M., 2011, "Effects of H_2 Enrichment on Flame Stability and Pollutant Emissions for a Kerosene/Air Swirled Flame With an Aeronautical Fuel Injector," Proc. Combust. Inst., **33**(2), pp. 2927–2935.
[17] Miniero, L., Pandey, K., De Falco, G., D'Anna, A., and Noiray, N., 2023, "Soot-Free and Low-NO Combustion of Jet A-1 in a Lean Azimuthal Flame (LEAF) Combustor With Hydrogen Injection," Proc. Combust. Inst., **39**(4), pp. 4309–4318.
[18] Dave, K., Link, S., De Domenico, F., Schrijer, F., Scarano, F., and Rao, A. G., 2025, "Kerosene-H_2 Blending Effects on Flame Properties in a Multi-Fuel Combustor," Fuel Commun., **23**, p. 100139.
[19] Singh, S., Amerighi, M., Scopolini, N., Andreini, A., Harth, S. R., and Trimis, D., 2025, "Effect of H_2 and Jet-A1 Fuel Split on Flame Stability and Pollutant Emissions From Low-Swirl Burner," Proc. Combust. Inst., **41**, p. 105858.
[20] Alabaş, H. A., and Çeper, B. A., 2024, "Effect of the Hydrogen/Kerosene Blend on the Combustion Characteristics and Pollutant Emissions in a Mini Jet Engine Under CDC Conditions," Int. J. Hydrogen Energy, **52**, pp. 1275–1287.
[21] Fu, P., Wang, Y., and Hou, L., 2024, "Numerical Study on Combustion of a Novel Micromix Multi-Nozzles for Kerosene/Hydrogen Fuels," ASME Paper No. GT2024-126048.
[22] Palanti, L., Mazzei, L., Bianchini, C., Link, S., Dave, K., de Domenico, F., and Rao, A. G., 2024, "CFD-Based Scouting for the Design of a Multi-Fuel Kerosene/Hydrogen Atmospheric Burner," 34th ICAS Congress, Florence, Italy, Sept. 9–13, Paper No. ICAS 2024-0432.
[23] Buro, S., Eggels, R. L., Nicolai, H., and Hasse, C., 2026, "Development and Assessment of Dual-Fuel Capabilities in Next-Generation Aero-Engine Injectors for Hydrogen and Liquid Fuels," ASME J. Eng. Gas Turbines Power, **148**(4), p. 041016.
[24] Xing, J., An, Z., and Kurose, R., 2024, "Analysis and Flamelet Modeling of Preferential Evaporation in SAF/Jet A Spray Flames," Proc. Combust. Inst., **40**(1–4), p. 105707.
[25] Sattelmayer, T., Mayer, C., and Sangl, J., 2016, "Interaction of Flame Flashback Mechanisms in Premixed Hydrogen–Air Swirl Flames," ASME J. Eng. Gas Turbines Power, **138**(1), p. 011503.
[26] Shamma, M., Hoffmann, S., Harth, S. R., Zarzalis, N., Trimis, D., Koch, R., Bauer, H.-J., Langone, L., Galeotti, S., and Andreini, A., 2021, "Investigation of Adjacent Lifted Flames Interaction in an Inline and Inclined Multi-Burner Arrangement," ASME Paper No. GT2021-59941.
[27] Haglind, F., and Singh, R., 2006, "Design of Aero Gas Turbines Using Hydrogen," ASME J. Eng. Gas Turbines Power, **128**(4), pp. 754–764.
[28] Mahesh, K., 2013, "The Interaction of Jets With Crossflow," Annu. Rev. Fluid Mech., **45**(1), pp. 379–407.
[29] Turner, M. A., Paschal, T. T., Parajuli, P., Kulatilaka, W. D., and Petersen, E. L., 2021, "Resolving Flame Thickness Using High-Speed Chemiluminescence Imaging of OH* and CH* in Spherically Expanding Methane–Air Flames," Proc. Combust. Inst., **38**(2), pp. 2101–2108.

[2] https://doi.org/10.5281/zenodo.20071084

Downloaded from asmedigitalcollection.asme.org/gasturbinespower/article-pdf/148/12/121009/7633651/gtp-26-1251.pdf by KIT Library user on 11 November 2026